Mem. S.A.It. Vol. 93, 201

Memorie della

3DCaTM: a 3D Cadmium Zinc Telluride spectroscopic module for hard X- and γ-ray astronomy

E. Caroli[1], L. Abbene[3], A. Zappettini[2], N. Auricchio[1], G. Benassi[5], M. Bettelli[2], A. Buttacavoli[3], G. Gargano[4], S. Del Sordo[4], F. Principato[3], J B. Stephen[1], S. Zanettini[5], and N. Zambelli[5]

[1] Istituto Nazionale di Astrofisica – Osservatorio di Astronomia e dello Spazio, Via Battiferro 93, I-40139 Bologna, Italy, e-mail: ezio.caroli@inaf.it
[2] Consiglio Nazionale delle Ricerche–IMEM, Parco delle Scienze 37/A, 43124 Parma, Italy.
[3] Dipartimento di Fisica e Chimica, Università di Palermo, Viale delle Scienze, Ed. 17, I-90128 Palermo, Italy
[4] Isituto Nazionale di Astrofisica – Istituto di Astrofisica Spaziale e Fisica Cosmica, Via U. La Malfa 153, I-90143 Palermo, Italy.
[5] Due2lab S.r.l, Via P. Borsellino 2, I-42019, Scandiano, Italy.

Received: 23 Janruary 2022; Accepted: 25 May 2022

Abstract. In the hard X-/soft γ-ray energy band (10 keV-10 MeV), a number of primary astrophysical questions are still open, mainly due to lack of sensitivity of the present instrumentation. New detectors are required to fulfill all the stringent requirements arising from scientific objectives and as much as flexible to be suitable for very different space mission classes such as the appealing mini/micro/nano satellite based one (in single or in cluster configuration). High modularity and compactness are therefore mandatory for these new instruments. In this perspective, 3D CZT spectro-imagers developments represent a challenging frontier. In this activity, our group has reached promising results, but a step forward on device components we developed is required to increase their technology readiness levels. To fulfill this requirement, we started the realization of a fully operational 3D CZT spectro-imager module as a relevant demonstrator of the high performance that we can achieve with this technology in spectroscopy, timing, Compton imaging and polarimetry. This module rely on the development of CZT drift strip sensors read by an innovative digital system. This 3D CZT module could be envisaged as a basic block suitable to build high performance focal planes for broadband (50-600 keV) Laue lenses telescopes or compact Compton instruments for a high populated micro/nano satellite cluster missions. Herein we present the current development of this project, and in particular, the different subsystems necessary for the construction of the final prototype, together with the results achieved in the characterisation of the single 3D CZT response.

Key words. High energy astrophysics, CZT spectrometers, 3D position sensitive detector, digital pulse processing

1. Introduction

Hard X-/soft γ-ray astronomy is a crucial window for the study of the most energetic and violent events in the Universe as well demonstrated by past satellites (SAX, XTE), and still operating one's (INTEGRAL, Swift, NuSTAR). Despite the new and brilliant results obtained by these missions in the energy band between 10 keV and tens of MeV, there are still several unanswered scientific key questions such as: the origin of the 511 keV annihilation line from the Galactic Center region (Lingenfelter et al. 1989), the enigmatic shape of the high-energy spectra of AXPs and SGRs (Beloborodov 2013), the high-energy spectra of AGNs and their contribution to the high-energy Cosmic X-ray Background (Malizia et al. 2014), the physics and the origin of GRB's, and their relevance in cosmology (Kumara & Zhang 2015) and for gravitational waves electromagnetic counterparts (Guidorzi et al.2021).

Therefore, in the incoming decades, a big effort to overcome current limitations is required and new space instruments shall be developed both for deep observations of point sources and for serendipity events study and monitoring. These two types of observation require different instrument approaches: i.e. high sensitivity narrow field instruments, and wide field instruments able to observe a large fraction of the sky. Future telescopes implementing new high energy focusing techniques (such as broad-band Laue lenses) and new Compton detector are particularly challenging and promising (Tatischeff et al. 2016), Frontera & Von Ballmoos 2010)). These new instruments require detectors exploiting high dynamics to cover a large energy band and very high performance in terms of efficiency, spectroscopy, imaging and timing. In addition, the requirement to be suitable for a large class of satellites and different mission scenarios needs that these detectors have a high modularity and compactness.

CZT/CdTe room temperature technology, whose reliability in space has been already proven by several still operating satellite instruments, offers an efficient solution to fulfill at once all the above requirements by means of development of modular thick CZT spectrometers with spatial resolution in three dimensions. A straightforward application of 3D spectro-imagers in hard X-/γ-rays is the realization of advanced Compton detector that evaluate the incoming photon direction through the Compton kinematic reconstruction (Du et al. 2001).

Finally, we shall point out that 3D capabilities, associated with fine spectroscopy and fast timing, are essential to operate these detectors as high sensitive scattering polarimeters and open finally the possibility to perform highly reliable polarisation measurements of cosmic sources above 100 keV. These detectors, exploiting the drastic improvement (at least a factor 100) of sensitivity expected by the implementation of new high energy focussing optics such as broad-band Laue lens (Virgilli et al 2017), represent the key step to make polarimetry a standard observational mode, simultaneously with spectroscopy, imaging, and timing, in hard X/γ-rays astrophysics missions (Caroli et al. 2018).

2. The 3DCaTM Project objectives

The development of CZT spectrometers with spatial resolution in 3D represents a new challenging frontier that involves several international groups (Caroli & Del Sordo 2015). The reconstruction of the photon interaction positions in 3D allows the proper corrections from signal variations due to charge trapping and material non-uniformity, allowing to increase the sensitive volume of each detector unit without spectroscopic performance degradations. The adopted electrode configurations play both a key role to fulfill the requirements for each sensor unit and also limit the electronics readout channels. This configuration lies on the anodic strip drift structures (Kuvvetli et al. 2010).

In this perspective, we started the realisation of a demonstrator of a fully operational spectroscopic imager consisting of a detection module and a digital readout system. The detection module will finally be obtained by stacking four 20×20×6 mm^3 3D CZT drift

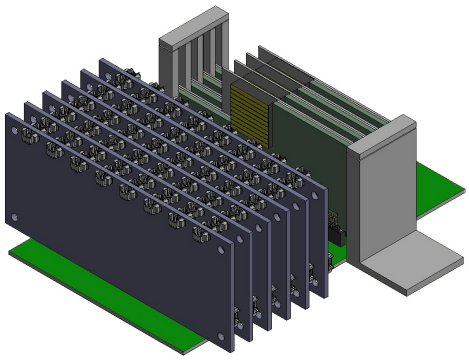

Fig. 1: Rendering of a possible configuration of the 3DCaTM detection module: the pack of the four 3D CZT sensors (at the right) with the charge sensitive front-electronics (six boards at left)

strip units, associated with a custom designed charge sensitive preamplification electronics for a total of 96 readout channels (Fig. 1). For the first time, a fully digital approach will be implemented in a 3D spectro-imager to exploit its performance in term of spectroscopy (< 1% FWHM at 511 keV), 3D spatial resolution (< 300 μm), polarimetry (Q > 0.5), timing (< 10 ns) and Compton imaging capabilities (< 10 degrees).

Large efforts have been made to develop a readout system implementing a digital pulse processing (DPP) approach, where the detector signals from charge sensitive preamplifiers are fed into fast digitizers and processed by using digital algorithms. These readout systems give many benefits against analog ones: e.g.: implementation of digital filters and procedures, stability and reproducibility, off-line and real-time signal analysis, multi-parameter analysis (arrival time, energy, pulse shape, etc.) for detector performance enhancements (Bolotnikov et al. 2014, Howalt Owe et al. 2019).

2.1. The 3D CZT sensor configuration

Our approach for the realization of this 3D CZT sensor rely on the simultaneously implementation of three ideas on the same semiconductor crystal:

- Planar Transverse Field (PTF) irradiation configuration, i.e. the optical axis of the sensor is orthogonal to the direction of the charge collection electric field (Fig. 2). This irradiation configuration allows increasing the photon absorption thickness (i.e. the detection efficiency) without impact on the charge collection efficiency, because the charge collecting distance can be maintained compatible with the charge mobility inside the material (up to 6/7 mm).
- The anode with a drift strip configuration (Kuvvetli et al. 2014), in which the signals from each collecting anode are readout separately, while the drift strip induced signals are readout in a grouped set, thus limiting the number of required electronics channels. The drift strip technique employs a number of strips (shown in brown color in Fig. 2) separating the anode readout strips (yellow). The drift strips are biased at decreasing voltage with respect to the anode one. The detector is biased such that the electrons generated by the photon interaction are drifted to a anode strip. This strips configuration modify the electric field inside the material so that the electrons are accelerated towards the anode while the holes, which have less mobility, have high probability to be trapped, not contributing to the final signal. Therefore the anode signal is nearly unaffected by the holes since the anode strips are screened by the bias strips. (van Pamelen & Budtz-Jørgensen 1997, van Pamelen & Budtz-Jørgensen 1998).
- The cathode is segmented into strips orthogonal to the anodic ones.

With this configuration, the CZT sensor can provide the 3D coordinate of hit caused by photon interaction using both the cathode and the anode side strips signals. The x direction can be determined using the collecting anode signals together with the grouped drift strip induced ones; the y direction is provided by the reconstruction of the interaction position between the two electrode using a combination of cathode and anode signal; the z position can

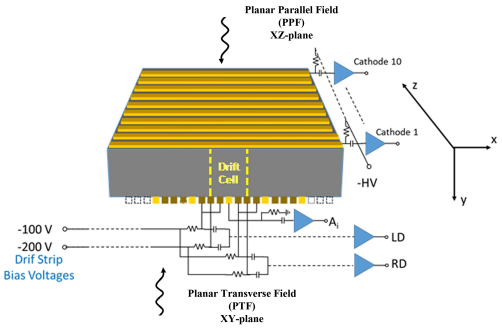

Fig. 2: (Drift strips anodic configurations and orthogonally segmented cathode bias and readout scheme

be derived weighting the cathode strip signals (Kuvvetli et al. 2014).

Tests performed with this type of configuration have confirmed that is possible to achieve fine spatial resolution, down to 0.3/0.4 mm) for all the three dimensions, i.e. by using only few tens of readout channels is possible to obtain a sensor segmentation equivalent to more than ten thousand voxels. In section 3 we will describe the technological process implemented for the realization of each 3D CZT unit.

2.2. The custom front end electronics

Each 3D CZT sensor unit needs 24 readout channels: 10 cathodes, 12 anodes, 2 groups of drift strips. These last two output signals are obtained by connecting in parallel the drift strips, which occupy the same relative position (left and right) with respect to a collecting anode. Therefore, to readout the full 3D CZT module we need 96 electronics channels. The 3D CZT module signal's readout is made by using a custom designed low noise charge sensitive preamplifier (CSP), implemented in a 16 channels hybrid board (3).

The current CSP boards design is the results of several laboratory prototypes and tests that have been designed to provide clean and stable signals to the digitizing electronics. With such a design a 500 keV event in the CZT arises a charge signal of 1 V. The main characteristics of the final CSP boards, which are biased at 5 V, are summarized in Table 1. In the 3DCaTM detection module each 3D CZT sensor unit will be plugged together distributing the six CSP cards (16 channels each) needed to readout the all channels to optimize the circuit layout.

Table 1: CSP main characteristics

Power/ channel	Decay time	Rise time	Gain	Noise (rms)
<90 mW	250 μs	0.2 μs	20	0.4 mW

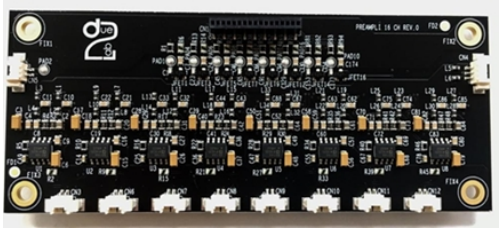

Fig. 3: The 16 channel CSP. Each surface of the hybrid board contains 8 CSP readout channels.

2.3. The digital readout system

A digital processing approach guarantees large flexibility of the detection system to different operative conditions: i.e. the detector performance can be tuned to the observational targets and space mission contest, without requiring change in its hardware. Recently, the group in Palermo developed an innovative Digital Pulse Processor (DPP) system for high resolution spectroscopic imaging (Abbene et al. 2015, Abbene et al. 2018).

This approach allows fine timing resolution and precise coincidence measurements ensuring a reliable selection of good scattered events improving the Compton kinematic reconstruction precision, i.e. a better background rejection and better imaging capabilities. Moreover, the possibility to preserve the pulses shape allows a fine analysis (*off-line*) of the charge sharing events and could provide a further en-

hancement of the achievable spatial and energy resolution.

The 3DCaTM project foresees that the almost one hundred preamplified channels will be sent to the input of a fast multi-channel digitization. The DPP system will rely on the use of two CAEN 64 channels devices (VX2740) equipped with 125 MS/s 14 bits digitizers and open FPGAs. The DPP implements a firmware based on two pipelined parallel shaping steps (Abbene et al. 2013): a fast and a slow shaping. The CSP output waveforms are shaped by using the classical single delay line (SDL) shaping technique. SDL shaping technique is very appealing for timing and pulse shape and height analysis (PSHA) at both low and high-count rates.

The group of University of Palermo has performed several tests by using 16 channels digitizing electronics (four CAEN DT5724 modules) and a CZT pixel detector. The digital system allows fine time coincidence analysis with coincidence time windows down to 10 ns, a feature that is very important for scattering polarimetry measurements and multiple events handling. In fact, with a time coincidence window of 30 ns, the DPP system is able to detect about 96% of the events in coincidence. In Section 5 we will discuss further results obtained with the developed DPP firmware in the evaluation of the spectroscopic performances achievable by 3D CZT sensors.

3. The 3D CZT sensors realisation

Each 3D CZT sensor is realized starting from a Redlen pixel detector made of spectroscopic graded CZT crystal of 19.6×19.6×6 mm^3 (Fig. 4(*left*)). The anode side is made by a set of 48 identical strips, 0.25 mm wide and with a 0.15 mm gap in between (Fig. 4(*centre*)). The set includes 12 collecting anode strips and 36 drift strips. The pitch between the collecting anode strips is 1.2 mm. Between each anode strip pair, there are three drift strips. The cathode side is also segmented in 10 strips of 2 mm pitch, 1.9 mm wide and with a 0.1 mm gap in between, placed orthogonally to anode strip (Fig. 4(*right*)).

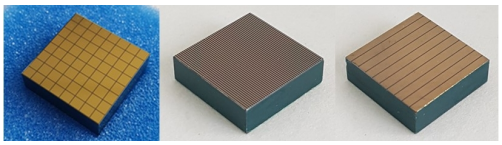

Fig. 4: (*left*) Original CZT crystal tile; (*centre*) final anode side configuration; (*right*) final cathode side configuration.

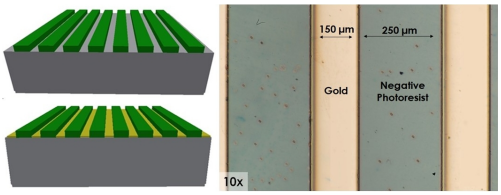

Fig. 5: (*left*) Lithographic patterning of photoresist layer on the anode side (top) and Au strips deposition using the resist mask pattern (bottom). The final resist thickness is 4 μm; (*right*) 10× optical microscope image of the CZT anode surface after the entire process

For the realization of the CZT 3D sensors, the IMEM/CNR group in Parma developed the following process:

1. Lapping, polishing, and cleaning of the CZT crystals, to remove original metallization on both cathode and anode sides and prepare CZT surface for the new electrodes;
2. Segmentation of cathode and anode, that requires a double patterning process on both sides of the CZT crystal;
3. Reduction of surface leakage current between the anode stripes by using special surface passivation techniques.

The minimisation of inter-strips leakage current is a critical requirement because the bias applied between each anode strip pair in operational conditions ranges up to several tens of Volts (ΔVs between 50-100 being the foreseen bias for correct drift cells polarization). A high surface leakage current can strongly affect the performance of the CZT sensor, both for spectroscopy and spatial resolution; thus we consider that a reasonable compliance value is < 5 nA at 50 V. Since the anode strips are 20 mm

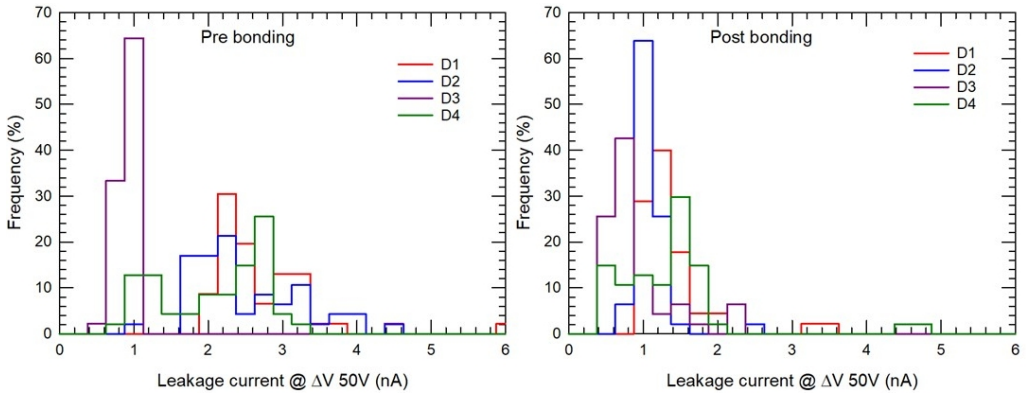

Fig. 6: The distribution of the leakage current between pair strips on the anodic side at δV=50 V: (*left*) on CZT sensor after the passivation and strip deposition process; (*right*) on drift strip CZT sensor after the bonding to the support.

long and very close, the fulfillment of such a requirement is a challenging technical step.

With other passivation techniques that have been used by IMEM/CNR in the past (for example wet passivation in 10%H_2O_2:H_2O solution, or deposition of Al_22O_3 thin layer), the surface leakage current between anode strips is around tens of nA (up to 50 nA) at 50 V (Zanettini et al 2018). Such leakage current value is too high to allow correct polarization of the detector. Therefore, an innovative surface passivation procedure has been developed and adopted implementing a two phases process, as represented in Fig.5(*left*): (i) Deposition of negative photoresist with anode pattern on the as-polished CZT surface; (ii) Deposition of Au strips by means of wet-chemical electroless technique from methanol solution (Benassi et al. 2017). Fig. 5(*right*) shows an optical microscope image of anode stripes at 10× magnification, which demonstrates the final results of the process.

The adopted process has reduced the surface dark leakage current by a factor 10 with respect to standard passivation techniques. Furthermore, the implemented passivation process has demonstrated both a high level of reproducibility over different CZT crystals and a good uniformity across the entire set of anode strips. Fig. 6(*left*) shows the measured surface leakage current distribution between adjacent strip pairs across the entire set of the anode side strips of the four 3D CZT sensors for a ΔV= 50 V, before bonding the sensor to its support.

Finally, each 3D CZT sensor has been mechanically attached and electrically bonded to an interface support, allowing the subsequent packaging of the four units to realize the proposed detector prototype. For this purpose, a custom support and electrical interface board has been developed. This support consists of five superimposed layers of different materials (Roger, Kapton and FR4) rolled together for a total thickness of 4 mm, i.e. thinner with respect to CZT crystal, and therefore allowing to minimize distance between sensor modules in the final prototype (Fig. 7). Each sensor is bonded to gold lines on the insulated Kapton film by inserting conductive glue in specific apertures of the flexi-cable. Bonding constitutes another very challenging technological step of the final prototype realization.

After bonding the 3D CZT sensors to the support, the leakage current measurements were repeated between the adjacent pairs of anodic strips in order to verify the impact of the process. Fig. 6(*right*) presents the distribution of these currents for each module. The bonding process has been successfully carried out for the four sensors and final leakage current values are slightly lower than pre-bonding values, typically <2 nA (in average 1 nA) at 50 V

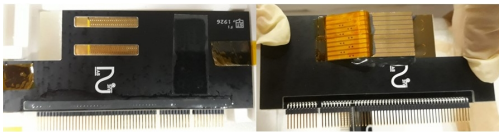

Fig. 7: The 3D CZT sensor support, and electrical interface: (*left*) anode side; (*right*) cathode side with the 10 Au lines on Kapton film used for bonding still folded, before final connection.

and <3 nA at 100 V. More than 75% of each distribution is within ±0.5 to ±1 nA from the mean. The improved uniformity across the anode strips set is likely a result of the more reliable electrical connection provided by the conductive epoxy connection with respect to the connection made with probe station tips during the pre-bonding measurements.

4. Response uniformity of the 3D CZT sensors

Before their implementation in the final 3DCaTM prototype, all the 3D CZT sensors have been characterized in their basic spectroscopic performances in term of Collection Charge Efficiency (CCE/Gain) and energy resolution (FWHM) using radioactive sources (^{241}Am, ^{57}Co, and ^{137}Cs) and a standard spectroscopic analogue readout chain composed by a spectroscopic amplifier and a 12bit multichannel analyzer. For these measurements we use a custom realized light-tight box (Fig. 8), suitably dehumidified with a membrane system, inside which the 3D CZT sensors can be installed one by one. The box contains both the power supply circuit and the preamplifier electronics to read the three adjacent central anodic cells. The characterisation of each 3D CZT unit was performed by measuring only the response of central anodic cell as a function of energy, with the main purpose of determining the response uniformity of the four sensors to verify both reliability and reproducibility of the manufacturing technique.

The detector is installed inside so as to be perpendicular to the surface of the box. In this way, it is possible to irradiate the 3D CZT sensor on the surface between the two electrode

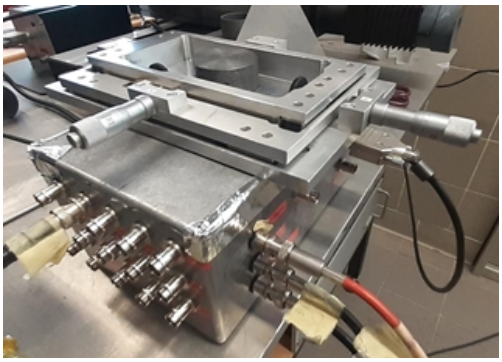

Fig. 8: Perspective view of the 3D CZT sensor box with the *xy* micro-metric tables, used to move the radioactive sources across the cathode-anode direction, on the top.

planes, that is in what we call PTF configuration. The radioactive sources inserted in a lead container with a 0.5 to 1 mm diameter outlet hole, depending on the source, were positioned using a micro-metric *xy* tablet (Fig. 8). In particular, we chose three positions respectively at about 5, 3, 1 mm respect to the anodic surface. In the following, these three positions will be referred to as *Yc* (cathode), *Ym* (centre), *Ya* (anode), respectively. In each of these three positions we acquired an energy spectrum with long integration time (600 to 4200 second), depending on the radioactive source flux and on the lead container hole used, to obtain a good counting statistic under the full energy peaks.

As an example, Fig. 9 shows the energy spectra measured for the 3D CZT unit D4 irradiated in PTF in the three source reference positions. with a ^{137}Cs source through a 0.5 mm diameter hole. Since the main purpose of these measurements was the evaluation of the uniformity of the spectroscopic response of the four 3D CZT sensors, we carried out, on each acquired spectra, the best fit of the full energy peaks of the different radioactive sources in the three reference positions to obtain the peak channel value (related to gain/CCE) of the sensor, and its FWHM (%) width, i.e. the energy resolution (Jeansonne & Foley 1991).

These two parameters were used to build the response linearity and the energy resolution as a function of the energy for each sensor and

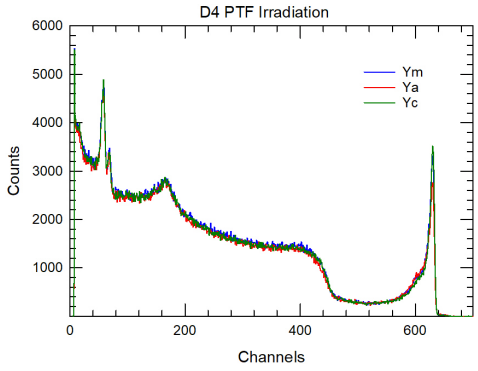

Fig. 9: Energy spectra in all the three reference positions obtained with 3D CZT unit D4 irradiated by a ^{137}Cs radioactive source.

for each source reference position. As an example, Fig. 10(*left*) shows the gain linearity vs energy between 20 and 700 keV for the set of four sensors, together with the best fit straight line for the central source position *Ym*. For the response linearity the measurements showed that the deviation is only a few percent (<5%) over the entire energy range and for all the sensors. Similarly Fig. 10(*right*) shows the evaluation of the energy resolution. The FWHM (%) estimated values for each sensor have been fitted twice with a two-parameter power law considering all the reference energies, and excluding the 22 keV line data, respectively. For all the fit we use a weighted procedure with $w=1/\sigma^2$, where σ is the estimated standard deviation.

Finally, using all the gain and resolution data obtained from the analysis described above, it was possible to evaluate the uniformity of the intrinsic spectroscopic response of the full 3D CZT sensor set before proceeding to the subsequent tests with the digital readout system and final implementation in the demonstrator prototype. Figure 11(*top*) shows the distributions of the gain uniformity in the three positions for all the sensors. Here, ΔPeak(%) is defined as $(P_i-\langle P\rangle)/\langle P\rangle \times 100$, where P_i is the peak channel at the *i-th* energy and <P> represents the weighted average over the four sensors at the same energy. These results clearly show that, despite the severe limitations of the *collimators* used and the inaccuracy of the alignment system, a significant difference is observed in the distribution among the three positions in PTF irradiation (see section 5). At the anode position the distribution widens and flattens to within ±4%, while in the other two positions (centre and cathode) it remains confined within ±1%, even if more spiked for the position close to the cathode.

Similarly, Fig. 11(*bottom*) shows the distributions of the ratio values obtained dividing the FWHM(%) evaluated at each reference energy and for each sensor by the weighted FWHM(%) average (<FWHM>) at each energy over the four 3D CZT sensors. These ratios have been calculated separately for all the three source positions (*Ya*, *Ym*, and *Yc*) used in PTF irradiation measurements. The distributions presented in Figure 13 do not highlight significant differences in shape and width between the various positions. In particular, all the distributions have a width (FW10%) compatible with an overall dispersion confined within 20%.

5. Spectroscopic performance of the 3D CZT sensor

In the 3D CZT sensor, the complex strip electrode structure and the effects of physical processes occurring in CZT detectors (charge sharing, charge trapping) give rise to charge pulses with different features and shapes. The charge collected on an electrode is related to the variation of the weighting potential between the charge generation and collection points. The presence of monotonic and non-monotonic weighting potentials often creates pulses with different shapes, strongly depending on the generation positions of charge carriers and their trajectories.

The wide variety of collected and induced-charge pulses in a CZT drift strip detectors is mainly represented by the following pulse classes (Fig. 12): (i) collected-charge pulses arising from charge carriers collection at one electrode; (ii) induced-charge pulses, with zero-saturation level, induced in drift strips by photon interactions near the cathode and related to the electron charge drift; (iii) induced-

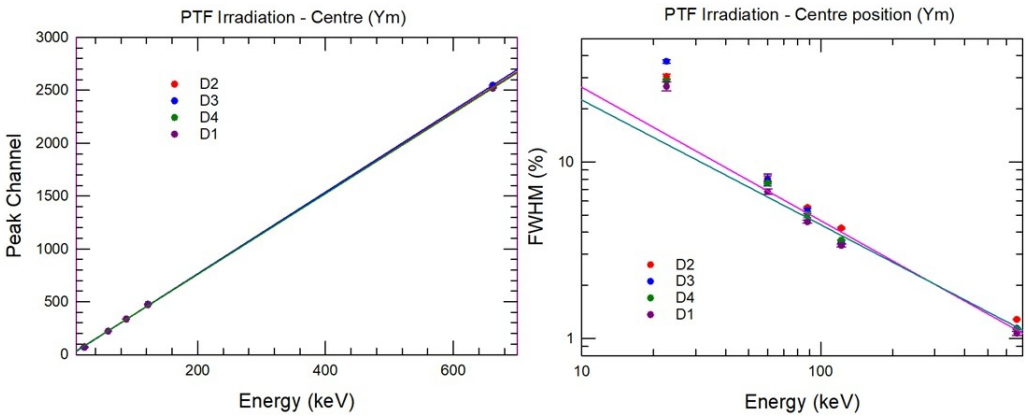

Fig. 10: (*left*) Response linearity. The graph shows the positions of the reference energy peaks as a function of the energy for all the 4 sensors irradiated in PTF with the source in the *Ym* position (centre). Estimated errors on the peak channel values are much smaller than the symbol size, i.e. always a fraction of channel up to 661 keV, where the one σ error slightly exceeds one channel; (*right*) The plot reports the evaluated resolution (FWHM (%)) for each reference energy peak as a function of energy for all the 4 sensors. The pink continuous line is the model obtained by fitting simultaneously all the data for the 4 sensors by a power law, while the dark cyan line is the model obtained excluding the 22 keV FWHM estimations.

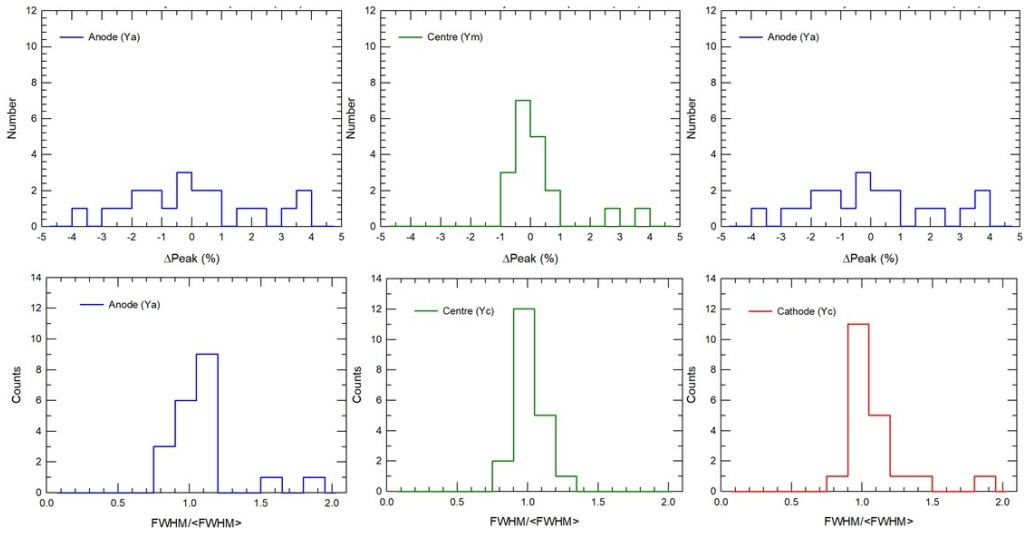

Fig. 11: The distribution of the percentage variations with respect to the average value (at each reference energy) of the peak channel (*top*) and of the ratio between the FWHM(%) and the weighted average values at each energy (*bottom*) over the full set of sensors, in the three reference source positions (*Ya*, *Ym*, *Yc*)

charge pulses, with negative and positive saturation levels, induced at the the drift strips, by photon interactions near the anode.

For the spectroscopic performance evaluation of each 3D CZT module we used the single module test box shown previously in Fig. 8. In these measurements the CSPs sig-

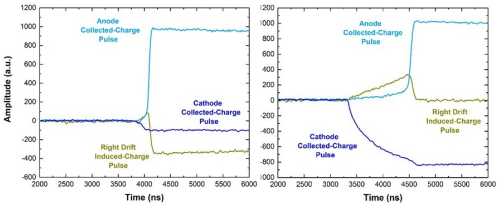

Fig. 12: A sample of measured pulses from anode, cathode and drift strips. Left plot shows signals generated by a photon interacting close to anode, while the right one for a photon interaction close to cathode. Cyan and blue plots refer to collected-charge pulse signals class (i), while green lines are representative for induced-charge pulses with zero-saturation signals type (ii) in the right panel, and for induced-charge pulses with positive- and negative-saturation levels signals type (iii) in the left one.

nals were read and processed by a 32-channel digital electronics based on eight digitizers (CAEN DT5724, 16 bit, 100 MS/s) driven by an original firmware (Abbene et al. 2015, Gerardi et al. 2014). The data from each channel are transmitted, through USB, to PCs, where the user can control both the acquisition and the analysis. Due to the complex analysis required by the different pulse shapes, we performed, at this step, a mixed *on-line/off-line* pulse processing. For each CSP output channel, the digital system performs *on-line* pulse detection, time-tag triggering and provides to the PCs a sequence of selected pulses (Snapshot Waveform) with the related arrival times. Therefore, the data produced by the digital system was *off-line* processed with dedicated analysis taking into account the different features of collected-charge pulses and induced-charge pulses. The final product of the *off-line* analysis are the height (i.e. the photon energy), the saturation levels (contribute induced by trapped charges) and the peaking time of the signal pulses.

The spectroscopic response of the single 3D CZT module was investigated by using radioactive calibration sources (^{241}Am: 59.5 and 26.3 keV; ^{57}Co: 122.1 and 136.5 keV; ^{137}Cs: 661.7 keV). All measurements were performed at T = 25°C, and in both irradiation modes: PTF and PPF (Photon Parallel Field, i.e., through the cathodic surface). Figure 13(*left*) shows the measured 662 keV photopeaks of uncollimated ^{137}Cs spectra for a collecting anode strip at different cathode bias voltages. The drift strip bias voltages of -100 V for adjacent drift strips and -200 V for central drift strips represent the best compromise found between charge collection improvements and leakage current increasing. The results clearly highlight as the best energy resolution was obtained at low cathode voltage values (-350 V). This is due to the particular electrode structure of the detector: once the drift strip voltages are fixed, higher cathode voltages worsen the electron charge collection on the collecting anode. We obtained spectra with excellent energy resolution of 1.3% FWHM at 661.7 keV without any corrections for charge sharing or trapping.

This is a key result, confirming the important technological progress obtained in fabrication of our CZT drift strip detectors. Typically, energy resolution of 3-4 % at 662 keV were obtained from uncollimated raw ^{137}Cs spectra measured with other CZT drift strip prototypes (Budtz-Jørgensen et al. 2017, Howalt Owe et al. 2019). Fig.13(*right*) shows uncollimated ^{57}Co spectra measured by using the PTF and PPF geometries. At lower energies the PPF geometry ensures better performance than the PTF one, thanks to charge generation occurring near the cathode side. In this case, the pulses are less sensitive to the holes contribution. However, at higher energies (^{137}Cs source), with charge generation points spanned over the overall cathode to anode distance, similar performance characterizes the two irradiation geometries, as reported in Table 2. In this case, the PTF geometry will ensure much higher detection efficiency over the 20 mm thickness.

A critical issue observed in 3D CZT drift strip detectors is represented by the presence of non-uniform spectroscopic response over the cathode-anode distance, with increasing degradation for photon interactions near the anode (Budtz-Jørgensen et al. 2017). These distortions are highlighted by the spectra shown in Fig. 13 from collimated ^{57}Co source (Pb collimator; ϕ=1 mm) irradiated in PTF geometry at three different positions between cathode

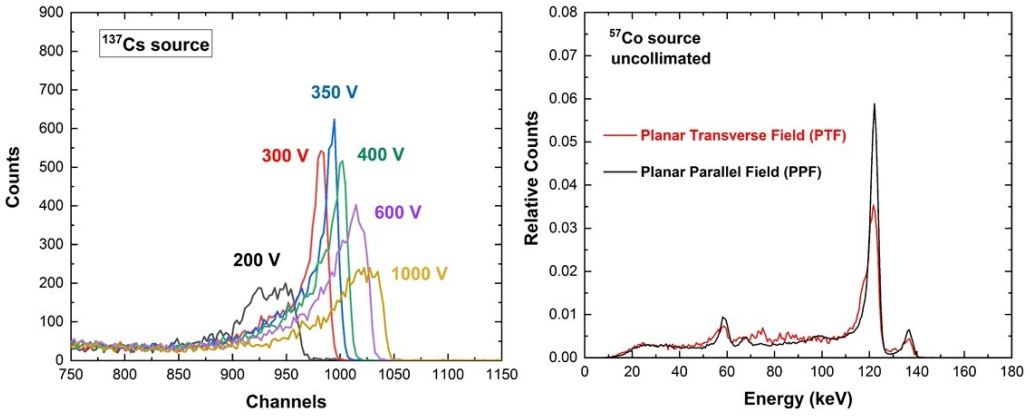

Fig. 13: (*left*) The spectra of the 662 keV photopeaks (^{137}Cs) measured from a collecting anode strip at different cathode bias voltages; (*centre*) Measured ^{57}Co spectra of a collecting anode strip in planar transverse field (PTF) and planar parallel field (PPF) geometry. Energy resolution of 4.9% and 3.3% FWHM at 122.1 keV; (*right*) Collimated ^{57}Co spectra of a collecting anode strip in PTF geometry at different irradiation positions.

Table 2: Energy resolution (FWHM) at different energies of a collecting anode strip of the 3D CZT drift strip detector in PTF and PPF irradiation geometries. The energy resolution values are referred to raw energy spectra with no spectral correction. The Fano noise was calculated by using a Fano factor F=0.1 (Devanathan et al. 2006).

	ΔE FWHM, keV (%)	
E (keV)	PTF	PPF
59.5	4.2 (7 %)	3.3 (5.6 %)
122.1	6.0 (4.9 %)	4.0 (3.3 %)
661,7	8.6 (1.3 %)	7.9 (1.2 %)

and anode. The photopeak centroid is reduced by ~6% from the cathode to the anode side and the energy resolution worsens from 3.2% (near the cathode) to 7.5% (near the anode) FWHM. This is due to the weighting potential behaviour of the collecting anode that makes the pulses more sensitive to the holes contribution and, therefore, to their trapping effects.

Generally, a mitigation of these non-uniformity can be obtained through the analysis of some features of the cathode and the anode pulses. In our case the cathode to anode (C/A) ratio, the cathode peaking time and the electron drift time were estimated, with the goal to exploit their potentialities in performance recovery. The C/A ratio is widely used in CZT detectors for the compensation of these distortions (Bolotnikov et al. 2016, Yi et al 2013). However, some critical issues must be taken into account when C/A ratio is used in CZT drift strip detectors (Abbene et al. 2020).

First, the low cathode bias voltages (-350 V) creates significant fluctuations in C/A ratio values and problems in energy calibration of the cathodes. Here, the cathode calibration was successfully performed through low energy spectra (^{241}Am and ^{57}Co sources) measured in PPF geometry, obtaining quite good linearity. Second, charge sharing is present among the cathode strips and, therefore, charge sharing addition (CSA) is necessary to correctly estimate the total charge from cathode strips.

The peaking time of the cathode pulses also depends on the photon interaction position between cathode and anode; due to the similar peaking time values of the shared pulses, it can be helpful when CSA fails. The electron drift time is the time between the charge generation of the electron cloud until its collection at the anode strip. This is very helpful for dou-

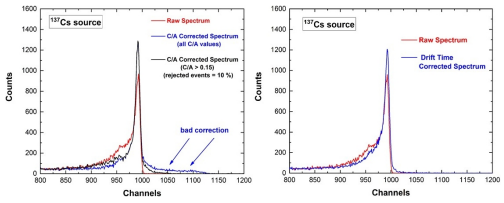

Fig. 14: Measured ^{137}Cs energy spectra corrected with: (*left*) C/A ratio correction (black and blue lines); (*right*) Drift time correction (blue line).

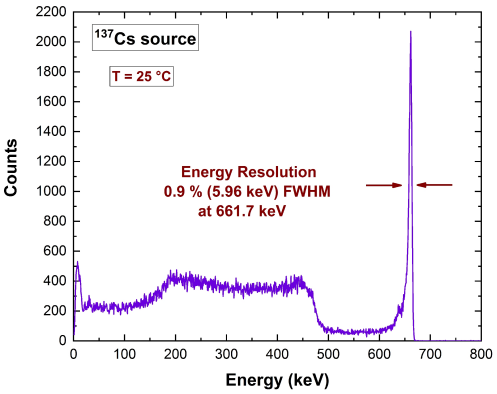

Fig. 15: Uncollimated ^{137}Cs energy spectrum from an anode strip after full spectral correction. The energy spectrum is obtained with the collecting anode events in temporal coincidence with all pulses from drift and cathode strips. The correction was only applied to the anode strip pulses in temporal coincidence with the induced-charge pulses with negative saturation levels.

ble event positioning of Compton interactions. The estimation of the drift time is strongly influenced by the correct measurement of the arrival times of the pulses that is more critical for the anode pulses, due to their slow leading edge for photon interactions near the cathode.

Taking into account all these parameters derived from the shape analysis of the digitized pulse, efficient and reliable spectral correction can be applied. The ^{137}Cs energy spectra after spectral correction (C/A and drift time) are shown in Fig. 14. Generally, the C/A correction gives slightly better energy resolution (1% FWHM at 661.7 keV) than the drift time one (1.16% FWHM at 661.7 keV). However, C/A correction requires the rejection of some C/A ratio values which give poor results (blue line of Fig. 14(*left*)), while drift time correction allows the analysis of all events.

Furthermore in devices like our 3D CZT sensor some induced-charge pulses from drift strips are characterized by negative saturation levels. Through simulation, we demonstrated that this saturation level is due to the charge induced by trapped holes. This fact opens the possibility to use this feature for reducing the effects of incomplete charge collection. The ^{137}Cs energy spectrum with the collecting anode strip events considered in temporal coincidence with all events from drift and cathode strips is shown in Fig. 15. The correction was only applied to the anode strip pulses in temporal coincidence with the induced-charge pulses with negative saturation levels. Excellent energy resolution of 0.9% FWHM at 661.7 keV characterizes the measured spectrum, this result representing currently the best energy resolution value obtained with 3D CZT drift detectors (Budtz-Jørgensen et al. 2017, Howalt Owe et al. 2019).

6. 3DCaTM: next steps

The measures presented confirmed that as regards the individual 3D CZT modules, the requisites envisaged in term of spectroscopic performances and replicability of the developed manufacturing technology are met, and different objectives set by the project have been achieved. The final phase began several months ago and is expected to arrive at the final demonstrator in two successive steps. The first step is the realization of a complete system for a single CZT 3D module and in a second phase the realization of the four-unit demonstrator. This first step was recognized, by the collaboration, necessary for two main reasons.

The first is closely related to the full characterization of the 3D spatial resolution of the 3D CZT modules, which currently is still missing. This characterization involves the use of finely collimated sources (0.1-0.2 mm). For this type of measurement we are trying to obtain time at ESRF (Grenoble) where a high energy (up to 500/700 keV) high flux

line (ID15A) is available. In parallel and as a backup, also taking into account the current difficulties in accessing ESRF due to the pandemic, the laboratories of the proposing groups are equipping themselves with sources and collimators suitable for carrying out tests of the same type at least for some energies (e.g. 137Cs). In both hypotheses, a single-sensor detection system allows a simpler set-up, with fewer constraints in terms of size and resources required and ensuring the same scientific results.

The second and more compelling reason is linked to the approval, at the end of 2019 by the H2020 / HEMERA program, of a technological payload (Caroli et al. 2019b) based on a 3D CZT module to be placed on a stratospheric balloon for a launch, currently scheduled for September 2022. This proposal was presented essentially to obtain information on the performance of these types of devices in a pseudo-spatial environment, and at the same time to verify the reliability of some technologies developed for the realisation of the 3D CZT sensors. The payload, which includes a detection system with a single CZT module, two 16 CSP hybrid boards built as part of the 3DCaTM project and a simpler 32-channel digital system, has been included in a contract funded by ASI (BAlloon Launched Detector for Gamma ray with 3 dimensional Resolution, BADG3R).

After the BADG3R flight and taking into account the result of the data analysis, we will proceed with the construction of the final 96-channel demonstrator (early 2023). With this system it will be possible to carry out very detailed measurements to validate the demonstrator as a significant prototype element in particular for the realization of high-performance focal planes for focusing instruments such as laue lenses telescopes capable of simultaneously operating as spectroscopic imagers and scattering polarimeters. We foresee to carry out this type of measurements by accessing external facilities such as ESRF and the LARIX at the University of Ferrara where the demonstrator could be tested directly in the Laue optics focus.

Acknowledgements. The present work was carried out as part of a project financed by ASI through the ASI-INAF agreement n. 2017-14-H.0 ”Studies for future scientific missions” A heartfelt thanks goes to our colleague and friend, Dr. Mauro Orlandini for his precious help in the LateX formatting of the manuscript.

References

Abbene, L., et al. 2013, NIM, A730, 124
Abbene, L. et al. 2015, J. Synch. Rad., 22, 1190.
Abbene, L. et al. 2018, J. Synch. Rad., 25, 257
Abbene, L., et al. 2020. J. Synch. Rad., 27, 1564
Beloborodov, A. M. 2013, ApJ , 762, 13
Benassi, G. et al. 2017, J. of Instrumentation, 12(2), 02
Bolotnikov, A. E. et al. 2014, IEEE TNS, 61, 787
Bolotnikov, A. E. et al. 2016, NIM, A895, 41.
Budtz-Jørgensen C.et al. 2017. IEEE TNS, 64, 1611.
Caroli, E. and Del Sordo, S. 2015, in Solid-State Radiation Detectors, S. Awadalla and K. Iniewski, eds., 83, CRC Press (Boca Raton)
Caroli, E. et al. 2018, Galaxies, 6(3), 69
Caroli, E., et al. 2019, IEEE NSS/MIC Conference Record, 9059948
Caroli. E. et al. 2019b, Proc. of 24th ESA Symp. on European Rocket and Balloon Programmes, ESA SP-742, 321
Devanathan, R. et al. 2006, NIM, A565, 637.
Cayrel, R., Du, Y.F. et al. 2001, NIM, A457, 203
Frontera, F. and Von Ballmoos, P. 2010, X-Ray Optics and Instrumentation, Special Issue, 215375
Gerardi, G. et al. 2014, NIM, A768, 46
Guidorzi, C. et al. 2021, Exp. Astron., 51, 1203
Howalt Owe, S. et al. 2019. J. Instrum. 14, C01020
Jeansonne, M. S., and Foley, J. P. 1991, J. of Chrom. Sci., 29, 258
Kumara, P. and Zhang, B. 2015, Physics Reports, 561, 1
Kuvvetli, I. et al. 2010, NIM, A624, 486
Kuvvetli, I. et al 2014, Proc. SPIE. 9154, High Energy, Optical, and Infrared Detectors for Astronomy VI, 91540X
Lingenfelter, R.M. et al. 1989, ApJ, 343, 686
Malizia, A. et al.2014, ApJ Letter, 782, 25L
van Pamelen, M. A. J. and Budtz-Jørgensen, C. 1997, NIM, A403, 390
van Pamelen, M. A. J. and Budtz-Jørgensen, C. 1998, NIM, A411, 197
Tatischeff, V. et al. 2016, SPIE Proc. on “Space Telescopes and Instrumentation: Ultraviolet to Gamma Ray”, 9905, 99052N
Virgilli, E. et al. 2017, JATIS, 3(4), 044001
Yi, Y. et al. 2013. IEEE TNS, 60, 9
Zanettini, S. et al. 2018, IEEE NSS/MIC Conference Record,1